ASTRONOMICAL DATA ANALYSIS SOFTWARE AND SYSTEMS XIV
ASP Conference Series, Vol. 347, 2005
P. L. Shopbell, M. C. Britton, and R. Ebert, eds.

Processing of 24 Micron Image Data at *Spitzer* Science Center

Frank J. Masci, Russ Laher, Fan Fang, John W. Fowler, Wen Lee, Susan Stolovy, Deborah Padgett, and Mehrdad Moshir

Spitzer Science Center, California Institute of Technology, Pasadena, CA 91125, Email: fmasci@ipac.caltech.edu

Abstract. The 24μm array on board the *Spitzer* Space Telescope is one of three arrays in the Multi-band Imaging Photometer for *Spitzer* (MIPS) instrument. It provides $5'.3 \times 5'.3$ images at a scale of $\simeq 2''.5$ per pixel corresponding to sampling of the point spread function which is slightly better than critical ($\simeq 0.4\lambda/D$). A scan-mirror allows dithering of images on the array without the overhead of moving and stabilizing the spacecraft. It also enables efficient mapping of large areas of sky without significant compromise in sensitivity. We present an overview of the pipeline flow and reduction steps involved in the processing of image data acquired with the 24μm array. Residual instrumental signatures not yet removed in automated processing and strategies for hands-on mitigation thereof are also given.

1. Introduction

Since the launch of *Spitzer* in August 2003, observations with the MIPS-24μm array have enormously extended our understanding of the infrared Universe. The array has attained sensitivities $\simeq 1.5$ times better than pre-launch estimates (see Rieke et al. 2004 for a review), allowing imaging of star forming regions and high redshift galaxies to sensitivities and spatial resolutions approaching factors of $\simeq 10^3$ and $\simeq 10^2$ respectively better than *IRAS*.

The MIPS-24μm array is a 128×128 pixel Si:As Blocked Impurity Band (BIB) detector and operates in a broad spectral band extending from 21 to about 27μm. Pixels are continuously and non-destructively read out every $\simeq 0.52$ sec over possible integrations ranging from $\simeq 3$ to 30 sec. Due to bandwidth restrictions, the individual samples are not downlinked. Instead, a line is fitted to the ramp samples for each pixel using an on-board linear regression algorithm. The data frames are downlinked in units called Data Collection Events (DCEs) and are packaged by the Multi-mission Image Processing Laboratory (MIPL) into two-plane FITS cubes. The first plane contains the fitted slopes for each pixel and the second, the difference between the first two reads in the ramp, referred to as the first-difference. The first-difference frame effectively increases the dynamic range for slopes derived from ramps which saturate. To further limit data volume, only first-difference values which exceed a nominal threshold (set by the saturation level) are retained and downlinked.

The 24μm array has two data-taking modes. That just described is called "SUR" (for Sample-Up-the-Ramp) and is the primary science mode for this array. The second mode is called "RAW", where all ramp samples are downlinked and received as multi-plane FITS cubes. RAW-mode is only used for engineering purposes. All raw pixel data are represented in signed 16-bit integer format,

with SUR-mode data in units of Data Number/read-time (DN/read) and RAW-mode in DN. The popular observing mode is scan-map[1] mode, and results in the highest data volume with typically 11,000 DCEs downlinked per day for the 24μm array alone.

To process such large data volumes, an infrastructure of automated pipelines, running on a cluster of 34 CPUs has been set up at Caltech's *Spitzer* Science Center (SSC) (e.g., Moshir 2001). This paper reviews the reduction steps used to process specifically MIPS-24μm SUR-mode science data at the SSC. A summary of instrumental residuals not yet corrected in automated processing, and which may appear in products distributed to observers, is also given.

2. Pipeline Infrastructure Summary

Raw images undergo several stages of automated processing at the SSC to produce the best calibrated products. The SSC is responsible for archiving, distributing data to observers, and maintaining current information on instrument calibration. For the MIPS-24μm array, eight separate pipelines have been developed for the removal of instrumental artifacts at the DCE level, each specific to the particular data collection mode or flavor of calibration product needed. These are as follows:

1. SUR-mode *science* (input: two-plane FITS DCE of slope and difference).
2. RAW-mode *science* (input: multi-plane FITS DCE of sample reads).
3. SUR-mode dark-current *calibration* (input: ensemble of DCEs).
4. RAW-mode dark-current *calibration* (input: ensemble of DCEs).
5. Electronic non-linearity *calibration* (input: ensemble of RAW-mode DCEs).
6. Flatfield (non-uniformity) *calibration* (input: ensemble of SUR-mode DCEs).
7. Latent-image flagging (input: preprocessed ensemble of BCDs).
8. Pointing reconstruction and Final Product Generation (FPG) on BCD.

On ingestion of data, a pipeline executive ensures that calibration data are processed first, before being employed in the reduction of regular science DCEs. Calibration products are created from ensembles of input DCEs, and a procedural database query tool using a set of predefined rules has been developed (Laher & Rector, 2005). Calibration products are transferred to the science pipelines using database queries handled by a software module called CALTRANS (Lee et al. 2005). The main product resulting from a DCE is a Basic Calibrated Data product, or BCD, with raw pointing and distortion information attached to its FITS header. The final (Post-BCD) processing steps include pointing refinement using astrometric matching (Masci et al. 2004), and mosaicking of ensembles of BCDs to provide seamless final products (Makovoz et al. 2005). Post-BCD processing is not discussed in this paper.

For each processed 24μm science DCE, ten associated BCD image products are archived at SSC, a subset of which are distributed to users. The archived set includes uncertainty images, bit-mask images which summarize the processing status for each pixel (both for the slope and first-difference planes), and processing log files. For a full description, see the *MIPS Data Handbook*[2]. The above

[1]For a description of all modes, see http://ssc.spitzer.caltech.edu/documents/SOM/

[2]http://ssc.spitzer.caltech.edu/mips/dh/

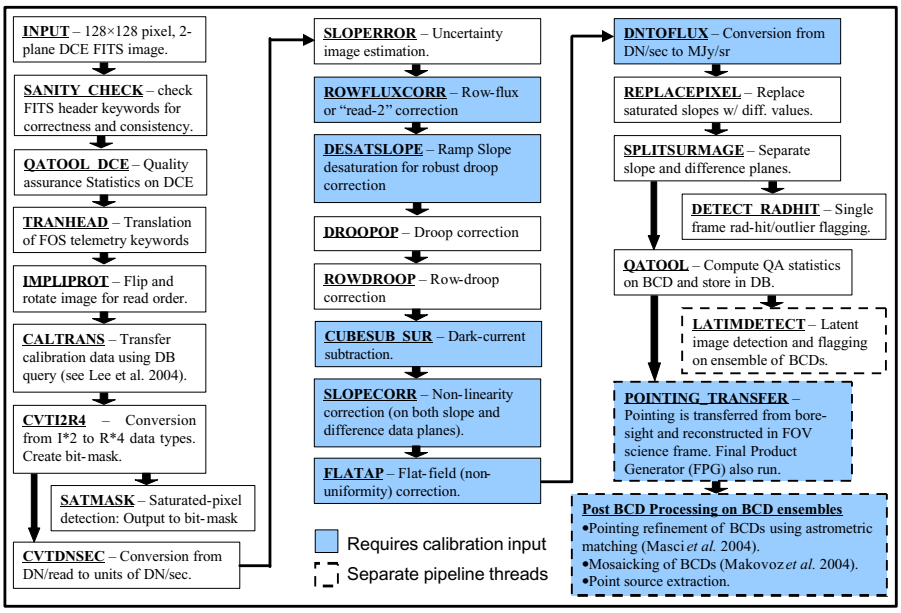

Figure 1. Processing flow in MIPS-24μm primary science pipeline.

suite of pipelines has also been implemented into offline stand-alone versions to facilitate testing and validation of algorithms before deployment in operations.

3. BCD Processing Summary

Figure 1 gives the ordering of reduction steps in the primary 24μm science pipeline. Processing algorithms were designed in collaboration with the MIPS Instrument Team. For a review, see Gordon et al. (2004). Here we give an overview of some of the more important reduction steps and instrumental signatures unique to the 24μm array.

The first step which modifies pixel values is CVTI2R4. This converts the signed 16-bit native raw image data into 32-bit floating point. This step also applies a truncation correction to the on-board computed slopes by adding a constant of 0.5 DN/read to every pixel in the slope plane.

The next step is detection and flagging of "soft" and "hard" saturated pixels (SATMASK). Soft saturation is where the samples saturate somewhere along the ramp, therefore biasing slope estimates. By saturation, we mean that the samples become pegged to the maximum value (+32768) as allowed by the on-board Analog-to-Digital Converter (ADC), which corresponds to $\simeq$ 30% full well. Soft saturated pixels are detected by simply thresholding pixels in the first-difference plane which are above a nominal value. For a 10 sec exposure, this value is $\simeq$ 3000 DN/read. Hard saturation is when the first sample, and all samples thereafter become pegged to the maximum ADC value. This is detected if both the derived on-board slope and first-difference are zero. Both soft and hard saturated pixels are flagged in a processing status mask and propagated downstream.

The SLOPERROR step initializes an uncertainty image using a robust noise model as applicable to slope data. This includes read noise, Poisson noise, and an estimate of the correlation between samples along a ramp from which the slope is derived. For a general overview of uncertainty propagation in SSC pipelines, see Moshir et al. (2003).

The ROWFLUXCORR step corrects a signature known as the "read-2" effect. This effect describes a bias introduced into the on-board slope measurement from a small additive offset in the second sample of every ramp. This offset is seen to vary across the array at the 0.2% level, primarily in the cross-readout (row) direction.

The DESATSLOPE is used to de-saturate slope pixels that were flagged for saturation from above (SATMASK). The de-saturated slope pixels are not propagated downstream. They are only used for robust computation of an effect known as "droop". Droop is an extraneous signal that is added to each pixel (at the $\sim$ 10% level) by the readouts. It is computed and removed by the DROOPOP module. Droop is directly proportional to the total number of counts on the array, including counts which are present above the ADC saturation level. For saturated pixels, slopes are underestimated, and thus for the purpose of computing droop, it is necessary to estimate slopes that would result from ramps which would continue beyond the saturation point. Slopes are de-saturated using the first-difference value and the non-linearity model. The ROWDROOP module corrects a second-order effect which similar to droop but whose signal in a pixel depends on the total signal from all pixels in its row.

The three standard calibrations are next. The dark current on each pixel is removed by subtracting a dark calibration image from both the slope and first-difference planes (CUBESUB_SUR). The dark calibration is computed by performing a symmetric outlier-trimmed average of a few hundred DCEs taken with the scan-mirror in the dark position. The dark current is small, and values range within 0-3 DN/sec. Correction for electronic non-linearity is performed by the SLOPECORR module. The non-linearity is accurately described by a quadratic up to ADC saturation, and the deviation from linearity is typically 10-15%. Flat-fielding is next (FLATAP). Flatfield calibrations exhibit maximum deviations of $\simeq$ 20% from flatness, and are primarily due to dark spots and low-level "blotchiness" in DCEs from absorption by debris on a pick-off mirror. The position and shape of these debris artifacts depend on the angle and scan-rate of the scan-mirror respectively. To correct for these, scan-mirror-dependent flatfields are created offline following each initial campaign processing run and deployed on the operations system before reprocessing of science data.

The final steps include flux-calibration (DNTOFLUX) and pixel replacement (REPLACEPIXEL). This last "pixel-modifying" step looks for all pixels that were flagged for saturation in the mask (from SATMASK), and replaces slope values with first-difference values in the *primary BCD product*. The original processed slope image (with no pixel replacement) is retained as an ancillary product.

4. Possible Instrumental Residuals

Broadly speaking, there are three instrumental signatures that may remain in 24μm BCD products after automated processing with the S11.0 version of SSC

pipelines. These can be ameliorated with further hands-on processing, although we expect to automate the corrections once they are sufficiently characterized.

The first residual may arise from inaccurate, scan-mirror dependent flat-fielding. As described above, the process is not yet fully automated. Mismatches between dark spot (debris-artifact) positions and corresponding actual mirror angles can occur. These mismatches lead to bright and dark residual patterns in BCDs, and given sufficient data, can be removed by re-creating flatfields from the BCDs and performing a self-calibration. For the most part, the scan-mirror-dependent flat-fielding is giving excellent results, although observers are encouraged to report anomalous cases to the SSC.

The last two residuals occur when bright, saturating sources are observed. The first is called "readout saturation" and occurs when a saturating cosmic ray or source depresses the output of a single readout channel. Since there are four readout channels, this gives the appearance of a "jail-bar" pattern. This has been characterized as a multiplicative effect and can be corrected by scaling the affected readout columns with a median of the other three unaffected readouts. This is only possible of course if the background doesn't show complex structure. The second effect is when the saturating source is bright enough to leave "dark" latents in many subsequent images. They appear dark because the slopes are fitted to saturated ramps, which turn out to be lower than average on the array. Given a sufficient number of frames with no complex structure, dark latents can be corrected by creating time-ordered sequences of self-calibration flats and dividing these into the BCDs.

Overall, the behavior of the 24μm array since launch can be described as excellent. Unless bright saturating sources are inadvertently observed, very few instrumental residuals are present. Future work will focus on reducing the residuals just described.

Acknowledgments. This work was carried out at the *Spitzer* Science Center, with funding from NASA under contract 1407 to the California Institute of Technology and the Jet Propulsion Laboratory.

References

Gordon, K. D., Rieke, G. H., Engelbracht, C. W., et al. 2004, PASP, (in press)

Laher, R., & Rector, J. 2005, in ASP Conf. Ser., Vol. 347, ADASS XIV, ed. P. L. Shopbell, M. C. Britton, & R. Ebert (San Francisco: ASP), 39

Lee, W., Laher, R., Fowler, J., Masci, F., & Moshir, M. 2005 in ASP Conf. Ser., Vol. 347, ADASS XIV, ed. P. L. Shopbell, M. C. Britton, & R. Ebert (San Francisco: ASP), 594

Makovoz, D., & Khan, I. 2005, in ASP Conf. Ser., Vol. 347, ADASS XIV, ed. P. L. Shopbell, M. C. Britton, & R. Ebert (San Francisco: ASP), 81

Masci, F. J., Makovoz, D., & Moshir, M. 2004, PASP, 116, 842

Moshir, M. 2001, in ASP Conf. Ser., Vol. 281, ADASS XI, ed. D. A. Bohlender, D. Durand, & T. H. Handley (San Francisco: ASP), 336

Moshir, M., et al. 2003, in ASP Conf. Ser., Vol. 295, ADASS XII, ed. H. E. Payne, R. I. Jedrzejewski, & R. N. Hook (San Francisco: ASP), 181

Rieke, G. H., Young, E. T., Engelbracht, C. W., et al. 2004, ApJS, 154, 25